AIAA JOURNAL
Vol. 42, No. 8, August 2004

Direct Simulation Monte Carlo Analysis of Thruster Plumes/Satellite Base Region Interaction

Jae Hyun Park* and Seung Wook Baek†
Korea Advanced Institute of Science and Technology, Daejon 305-701, Republic of Korea
and
Jeong Soo Kim‡
Korea Aerospace Research Institute, Daejon 305-333, Republic of Korea

The interaction of thruster plumes with satellite components is investigated, with emphasis on undesirable effects, such as disturbance force/torque, thermal loading, and species deposition in the Korea Multipurpose Satellite-II (KOMPSAT-II) base region. The actual configuration of the satellite is simplified by the consideration of four major components of hydrazine thrusters, the S-band antenna, and the surrounding ring. For the numerical simulation, a fully unstructured three-dimensional discrete simulation Monte Carlo (DSMC) code is developed and validated. The DSMC computation allows for examination of the detailed flowfield dynamics, as well as the wall conditions, which, otherwise, would not be possible from a simplified engineering analysis. The computations show that the present thruster arrangement used in KOMPSAT-II incurs a negligible disturbance force/torque and thermal loading compared with its nominal thrust/torque and solar heating. The simulations also indicate that the species deposition is insignificant due to the high surface temperature of the satellite body. Of the chemical species considered (H_2, N_2, and NH_3), more H_2 molecules collide with the S-band antenna cone. This study clearly shows the usefulness of DSMC calculations for analysis of plume effects in the development phase of a satellite.

Nomenclature

P_0	=	chamber pressure
q_{sol}	=	solar constant
r_{th}	=	radius of thrust throat
r_0	=	radius of thruster exit
T_0	=	chamber temperature
x, y, z	=	coordinates
Δt	=	time step
σ_T	=	thermal accommodation coefficient

Subscript

BOL	=	beginning of life

Introduction

SATELLITE motion is usually controlled by gas exhaustion from the thrusters into near-vacuum surroundings. Then, an undesirable interaction between plume and spacecraft body may cause considerable adverse effects such as disturbance force/torque, thermal loads, and contamination of sensitive equipment and sensors. Because these effects would result in a reduction of the satellite mission lifetime, their accurate modeling and predictions are very important at the design stage of a satellite.[1,2]

Received 16 April 2003; revision received 14 November 2003; accepted for publication 14 November 2003.

*Ph.D. Candidate, Division of Aerospace Engineering, 373-1 Kusung-dong, Yusung-ku; currently Postdoctoral Associate, Beckman Institute for Advanced Science and Technology, University of Illinois at Urbana–Champaign, 405 North Mathews Avenue, Urbana, IL 61801; jaepark@uiuc.edu. Member AIAA.

†Professor, Division of Aerospace Engineering, 373-1 Kusung-dong, Yusung-ku; swbaek@kaist.ac.kr. Senior Member AIAA.

‡Principal Researcher, Satellite Research and Development Division, Yusung-ku; currently Professor, School of Mechanical and Automotive Engineering, Sunchon National University, 315 Maegok, Sunchon, Jeonnam 540-742, Republic of Korea; jskim@suchon.ac.kr. Member AIAA.

The examination of the interaction between the exhausted plume and the satellite components through ground-based experiments is quite complicated and expensive, because it requires construction and operation of high vacuum facilities to reproduce the desired operating conditions, such as nozzle pressure ratio and Mach/Reynolds number at the nozzle exit. As a result, a numerical analysis is preferred. Among many numerical methods, the direct simulation Monte Carlo[3] (DSMC) technique is usually adopted for this kind of problem because the flowfield around a satellite involves a broad range of flow regimes, from the near continuum in the vicinity of the nozzle exit, through the transitional regime, to free-molecular flow in the region far from the nozzle.

Many researchers have investigated the fundamental characteristics of plume exhaust by comparing DSMC results with the experimental data.[1,4,5] However, recent studies concentrate more on the plume interactions in realistic spacecraft missions. Lumpkin et al.[6] and Rault[7] examined plume effects in the shuttle/Mir docking, whereas Giordano et al.[8] considered the x-ray multimirror mission (XMM) satellite. Gatsonis et al.[9] investigated the induced pressure environment incurred by the firing of small cold-gas altitude control thrusters onboard the suborbital environment monitor package (EMP) spacecraft. Other than the use of a DSMC method, a simplified plume analysis method[10] was developed earlier, based on the approximate relations[11–13] and continuum analysis. However, Markelov et al.[14] have pointed out that such an approach may cause low accuracy in the analysis of a practical complex system because it neglects some physical phenomena such as semishadow and multiple reflections.

Previous DSMC studies regarding satellites have usually focused on the nominal influences by the plume, rather than its undesirable side effects.[8,9] Given these factors, in the present study, the interaction between the thruster plume and the satellite base region is investigated by the use of the DSMC method, with emphasis on the estimation of plume disturbance effects. To deal successfully with the extremely complicated configuration of the satellite base region (in which the thrusters are installed and most exhaust gas mixture resides), a three-dimensional unstructured DSMC code is developed and validated through comparison with experimental data. It is then applied to the base region of the Korea Multipurpose Satellite-II (KOMPSAT-II) with firing thrusters. The exhausted plume interacts with various base region components such as the

dual thruster module DTM, S-band antenna, adapter ring, upper marmon ring, etc. Throughout this study, the flow structure inside the base region is investigated for diverse operating conditions, and the consequential dynamic and thermal disturbances are discussed. Based on the present numerical results, we can determine whether or not the DTMs are optimally arranged in the base region of the KOMPSAT-II.

KOMPSAT-II and Problem Definition

The KOMPSAT project is a Republic of Korea government program to establish the space technology of the Republic of Korea, starting from a mission of Earth observation. The first model (KOMPSAT-I) was already designed, manufactured, and successfully launched, and the upgraded second model (KOMPAST-II) is currently being developed. The overview of KOMPSAT-II is shown in Fig. 1a. The KOMPSAT-II propulsion system (PS) employs a 1.0-lbf (4.45 N) MRE-1 monopropellant hydrazine liquid rocket engine. The thrusting impulse is provided by the catalytic decomposition of monopropellant grade hydrazine (N_2H_4) in a propellant tank, and the combustion products, therefore, consist of H_2, N_2, and NH_3. Its actual configuration is shown in Fig. 1b. Only the major components in Fig. 1b are considered in the DSMC computation, such as the S-band antenna, DTM, propulsion platform, upper marmon ring, and adapter ring. The exhaust plumes from the thrusters in the DTM interact with those satellite components. For an efficient generation of necessary thrust/momentum, each thruster is inclined to the xz plane (base plate) by 16 deg and is parallel to the yz plane. The exit plane of the thruster is tilted outward ($+y$ or $-y$) by 30 deg. Consequently, the angle between the base plate and the normal vector of the thruster exit plane is 14 deg. In this study, the flowfield in the KOMPSAT-II base region is obtained under various operating conditions by application of the DSMC method. Results from the computations are used to estimate and discuss the undesirable plume interaction effects, such as disturbance force/torque, thermal loading, and species deposition.

DSMC Method and Its Application

The basic algorithms in DSMC are well described by Bird.[3] In this study, a three-dimensional DSMC code is developed by the use of a fully unstructured grid system to deal with severe geometrical complexity in the satellite base region. The simulated particles are traced via the intersection between the particle trajectory and the faces of the computational cells being sought.[15] The variable hard sphere (VHS) model is used for molecular collision, whereas the no time counter (NTC) method is employed for collision sampling. For the calculation of internal energy exchange between

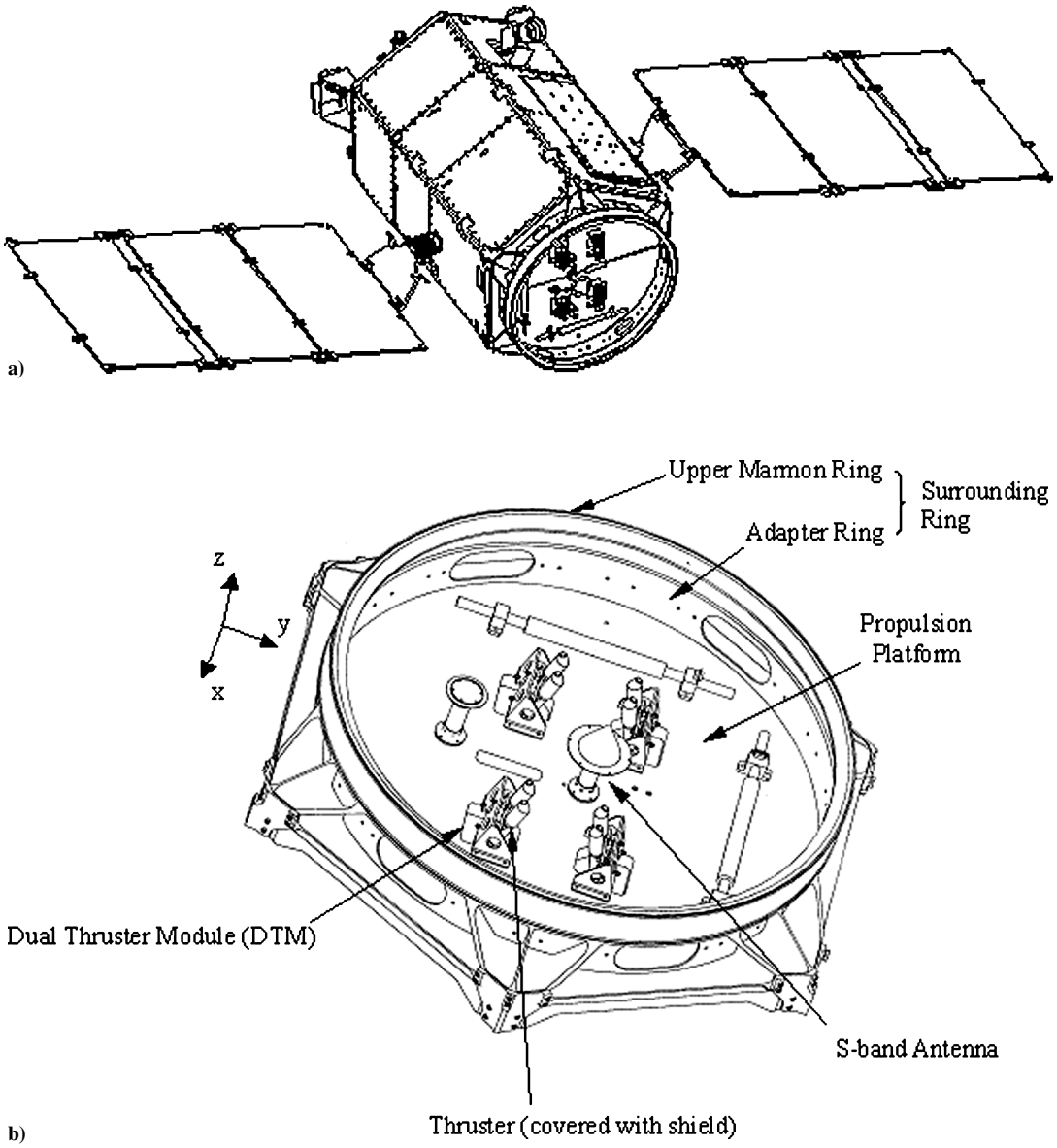

Fig. 1 Actual configuration of KOMPSAT-II: a) overview and b) magnified view of base region and major components therein.

the colliding molecules, the Borgnakke–Larsen phenomenological model is adopted. Because the medium temperature inside the base region is relatively low, rotational excitation is considered only, whereas chemical reaction and vibrational modes are neglected. This is justified because Kewley[16] reported that chemical reaction and vibrational energy became frozen just beyond the nozzle throat. The unstructured grid system is obtained from a commercial package called GRIDGEN[17] using the Delaunay technique. The cell size is carefully determined to be smaller than the local mean free path in every cell. The developed code is implemented on a personal computer cluster in which message passing interface[18] (MPI) and METIS[19] software are used for data communication between processors and domain decomposition, respectively.

Similar to previous work[20,21] the present code is validated through comparison with experimental data for a three-dimensional nitrogen plume impingement. The schematic of this problem is given in Fig. 2. For the DSMC computation, the inlet flow at the orifice is modeled as a uniform stream along the plume axis, in which negligible boundary-layer effects are assumed. The inlet properties are, therefore, calculated from isentropic relations for the stagnation conditions of 1000 Pa and 300 K. The impingement surface is modeled as a fully diffuse wall with full thermal accommodation ($\sigma_T = 1.0$), and the fully unstructured grid system is obtained from GRIDGEN. The typical computing conditions in this problem are as follows: grid cells = 30,000; number of particles = 100,000; transient steps = 150,000; and sampling steps = 5,000.

In Fig. 3, the present and previous DSMC results are compared with the experimental data for $\beta = 45$ deg. Figure 3 reveals three comparisons for surface pressure, shear stress, and heat flux distributions along the wall and shows strong a similarity between the present DSMC results, the experiments, and previously reported DSMC results.[21] Although not shown here, comparisons were also made for $\beta = 0$ and 90 deg, and the results were also found to be comparably accurate.

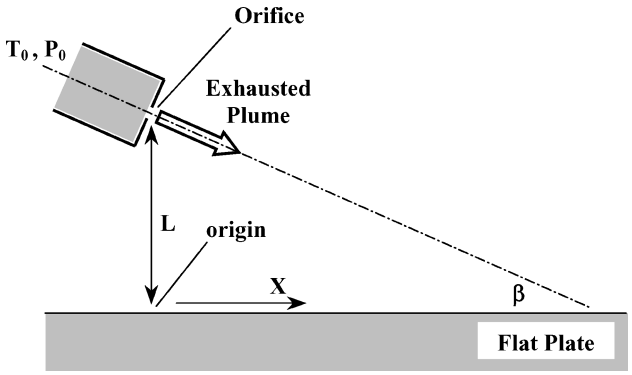

Fig. 2 Schematic of plume impingement problem.

Analysis by Engineering Method

Along with DSMC analysis, an engineering analysis was performed by ASTRIUM-France for the present problem.[2] Their approach follows the well-established classical plume analysis procedure.[22,23] The prediction of the plume effects by ASTRIUM in France consists of two steps: first, the plume flowfield visualization and second, the plume impingement calculation. The flowfield simulation begins with the analysis of the combustion chamber. The chemical compositions and physical properties are calculated under the assumption of thermodynamic as well as chemical equilibrium. The chamber pressure and temperature are computed as $P_0 = 9.8$ bar and $T_0 = 975$ K for the typical nominal thrust of 3.23 N and mass flow rate of 0.0015 kg/s, respectively.[24] The resultant mole fraction of H_2, N_2, and NH_3 are 0.664, 0.333, and 0.0377, as listed in Table 1.

The subsonic and supersonic flowfield inside the thruster nozzle is simulated by the solution of the axisymmetric Navier–Stokes equation. The medium is modeled as a single specie with averaged density and properties, based on equilibrium compositions. The vicinity of the nozzle exit is analyzed under the assumption of inviscid flow. Such an approach is known to be more suitable for a small thruster (less than 20 N in thrust) such as the MRE-1 in this study, rather than a method of characteristics (MOC) analysis. The accuracy of the Navier–Stokes and Euler solvers at ASTRIUM-France has already been confirmed through comparison of their numerical results with experimental data for various thrusters other than the 1.0-lbf monopropellant rocket engine. The continuum flow at the nozzle exit is expanded into space by a source flow method.[12,13]

Figure 4 shows the exit properties from the engineering method. These are also utilized as the thruster outlet conditions for the DSMC computation in the following section. Because the adiabatic condition is imposed on the nozzle wall, the temperature drastically increases across the boundary layer, whereas the axial velocity shrinks to zero. However, the density has its maximum near the edge of boundary layer, where the high velocity and the low medium temperature are observed. In correspondence with the density profile, the Knudsen number reaches a minimum there. When the grid system is generated for the particle simulation, the cell size at the vicinity of the thruster exit should be set sufficiently smaller than the local mean free path to guarantee good accuracy.

The flowfield properties resulting from the source point method in the first step are utilized as the input condition for the

Table 1 Chamber condition and species composition of combustion product for KOMPSAT-II thruster

Property	Value
Chamber pressure	9.8 bar
Chamber temperature	975 K
Operating thrust	3.23 N
Operating mass flow rate	0.0015 kg/s
Species composition	H_2:N_2:NH_3 = 0.664:0.333:0.0377

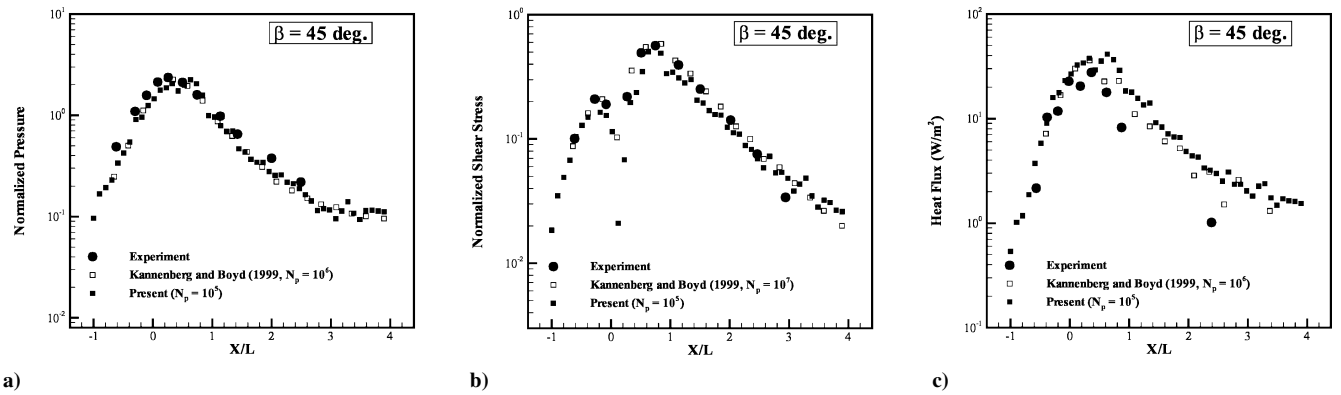

a) b) c)

Fig. 3 Comparisons between experiment, previous DSMC data,[21] and present DSMC result for plume impingement with β = 45 deg: a) surface pressure, b) surface shear stress, and c) surface heat flux.

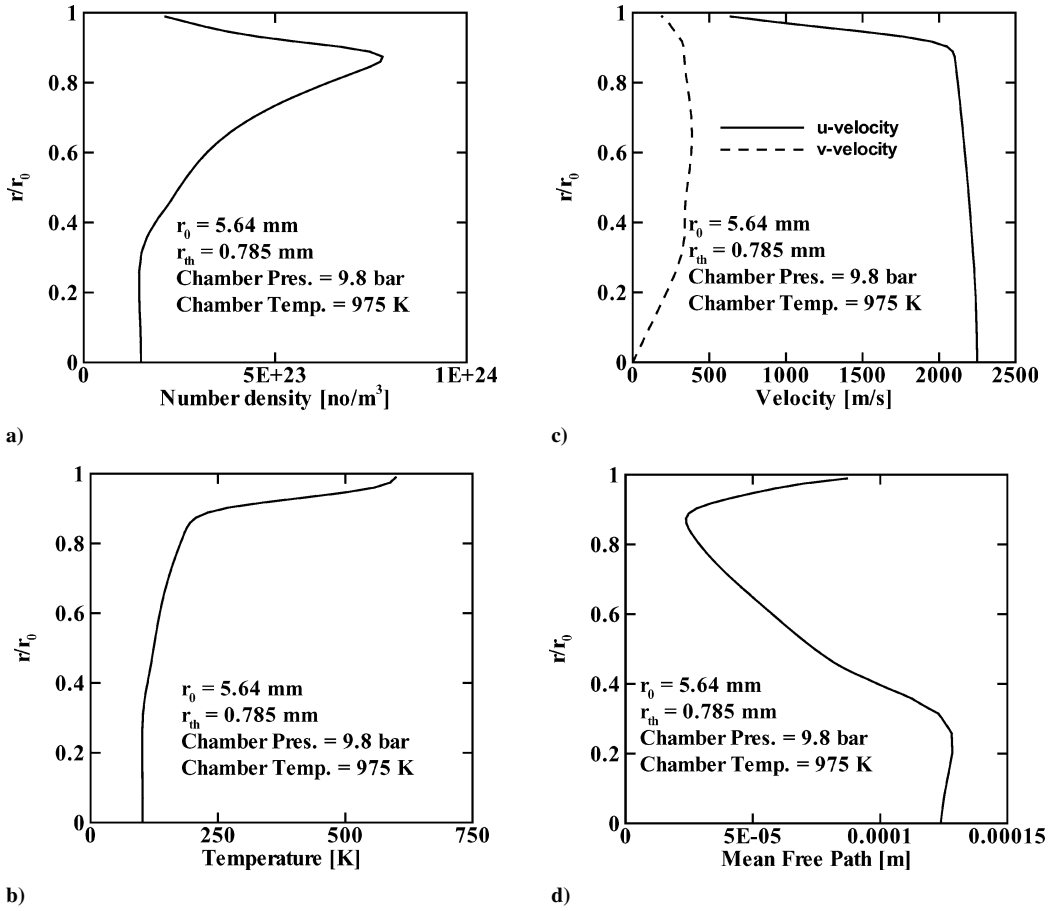

Fig. 4 ASTRIUM-France's results for nozzle exit properties of MRE-1 thruster at a given chamber conditions of P_0 = 9.8 bar and T_0 = 975 K (ASTRIUM-France analysis does not consider each species of combustion mixture, mean free path computed based on averaged density and molecular diameter of mixture): a) number density, b) temperature, c) velocity, and d) mean free path.

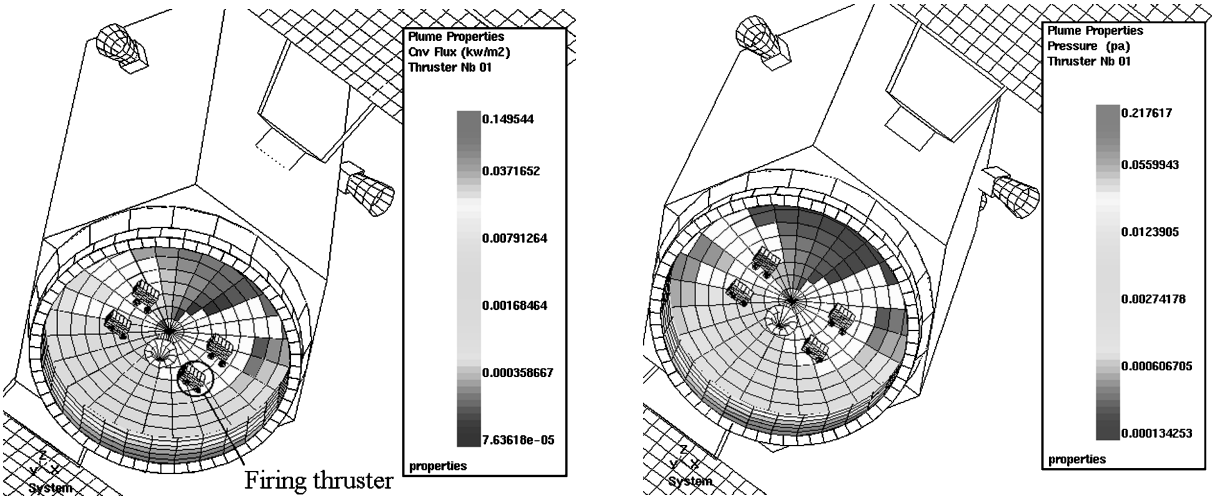

a) Wall heat flux **b) Wall pressure**

Fig. 5 Analysis by engineering method, only one thruster (inside circle) in on mode, others in off mode: a) wall heat flux and b) pressure distribution (in ASTRIUM-Frances analysis, base region of satellite simplified by considering four thruster modules, S-band antenna, and surrounding ring only; entire satellite body has not been taken into account in the computation).

DSMC estimation. Of course, the whole geometry is discretized into a number of elements. The gas stream at impingement is classified according to the local Knudsen number. Then, the force, mass flux, and heat transfer at the element are distinctively obtained from Newton's theory for the continuum regime, or the gas kinetic theory for free-molecular flows. If it is in the translational regime, a local bridging method is adopted.[11] Also, the total dynamic, thermal, and contamination effects are determined by summation of all of the elemental disturbance properties.

Figure 5 shows the distribution of wall heat flux and pressure caused by firing of a single thruster located in $x > 0$ and $y > 0$ of the satellite coordinate system. Higher pressure and heat flux are found only at some parts of the S-band antenna, surrounding ring, and base plate close to the on-mode thruster. The molecules emitted from the thruster keep traveling freely until they arrive at the solid

surface. Table 2 lists the disturbance force/torque and maximum wall heat flux when only one primary thruster in $x > 0$ and $y > 0$ is being fired. Disturbance force and torque are defined by

$$\boldsymbol{F}_{\text{disturbance}} = \int_{\text{surface}} \boldsymbol{f}\,\mathrm{d}S \tag{1}$$

$$\tau_{\text{disturbance}} = \int_{\text{surface}} (\boldsymbol{r} \times \boldsymbol{f})\,\mathrm{d}S \tag{2}$$

where $\boldsymbol{F}_{\text{disturbance}}$ is the total disturbance force over the KOMPSAT-II base region, $\boldsymbol{\tau}_{\text{disturbance}}$ is the total disturbance torque with respect to a given reference position, $\boldsymbol{f}$ is the force acting on the surface element, and $\boldsymbol{r}$ is the distance vector from the reference position. In the present study, the torque is computed with respect to beginning of life (BOL) mass center at the beginning stage of operation. Its position is given by $(x_{\text{BOL}}, y_{\text{BOL}}, z_{\text{BOL}}) = (-9.78, -1.92, -775.1)$ mm if the origin is set at the center of the base plate. The center of mass of a satellite changes during the mission due to the continuous consumption of propellant.

However, the engineering analysis may not be proper for a more practical situation like the simultaneous firing of multiple thrusters in rarefied surroundings, in which the plume/plume interaction and species separation would be significant.

Results and Discussion

The DSMC code validated in the preceding section is applied to the flowfield analysis for the KOMPSAT-II base region. For the numerical simulation, the actual configuration in Fig. 1 is simplified by choosing only the major equipment and structural parts such as the S-band antenna, adapter ring, upper marmon ring, propulsion platform, and four primary thrusters. Figure 6 presents the model configuration and its surface grid system used in this study. The undesirable plume effects on the satellite originate primarily from the plume/satellite interaction in the base region, whereas the contribution by outside molecules is negligible. Therefore, the surrounding vacuum does not have much involvement with the total computational domain. It is extended to just 0.9 m in radius, 0.1 m in depth, and 0.5 m in height from the base region of KOMPSAT-II. As a boundary condition, the surface temperature of each component in Table 3 is determined by the values at the worst condition during KOMPSAT-II maneuvering.[24] The worst condition corresponds to the coldest condition during the mission, such as when the satellite has the smallest solar heat flux, the smallest thermal absorption by the satellite surface, and the smallest heat dissipation through the electrical equipment. Because the operating altitude of KOMPSAT-II ranges from 670 to 700 km, the environment is assumed to be a vacuum. Consequently, all of the boundaries except for the solid wall are presumed as a particle sink in the DSMC computation. Numerical calculations are performed for four representative mission conditions, as listed in Table 4. In case A, all four thrusters are fired simultaneously to produce the maximum thrust, which corresponds to orbit transfer. The other cases, B, C, and D are made by a combination of two thrusters in on mode and the other two in off mode, to achieve the required attitude control motion of the satellite.

Table 2 Disturbance force/torque and maximum thermal loading from the engineering analysis by ASTRIUM-France[a]

Property[b]	x	y	z
Main thrust, N	0	−0.783	3.14
Disturbance force, N	3.97×10^{-3}	1.36×10^{-2}	1.69×10^{-3}
Main torque, N · m	−0.427	−0.596	−0.149
Disturbance torque, N · m	1.27×10^{-2}	-4.02×10^{-3}	1.65×10^{-3}

[a]Result is for case in which only one primary thruster in $x > 0$ and $y > 0$ is being fired.
[b]Maximum wall heat flux ≈ 150 W/m^2.

Table 3 Temperature of satellite components in the base region at worst case

Satellite component	Temperature, °C
S-band antenna	−33.0
Propulsion platform (MLI)[a]	−135.0
DTM (MLI)	−96.0
Upper marmon ring	−13.0
Adapter ring (MLI)	−122

[a]Multilayer insulation blanket (MLT).

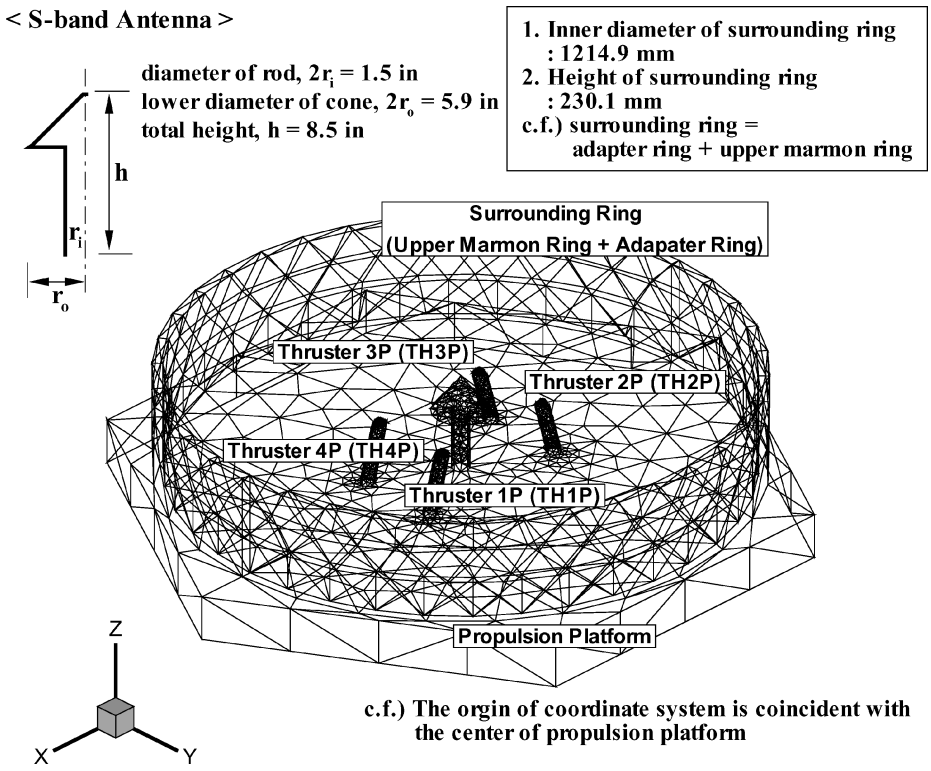

Fig. 6 Simplified configuration of satellite base region for DSMC simulation; schematic consists of triangular grid system on the satellite surface.

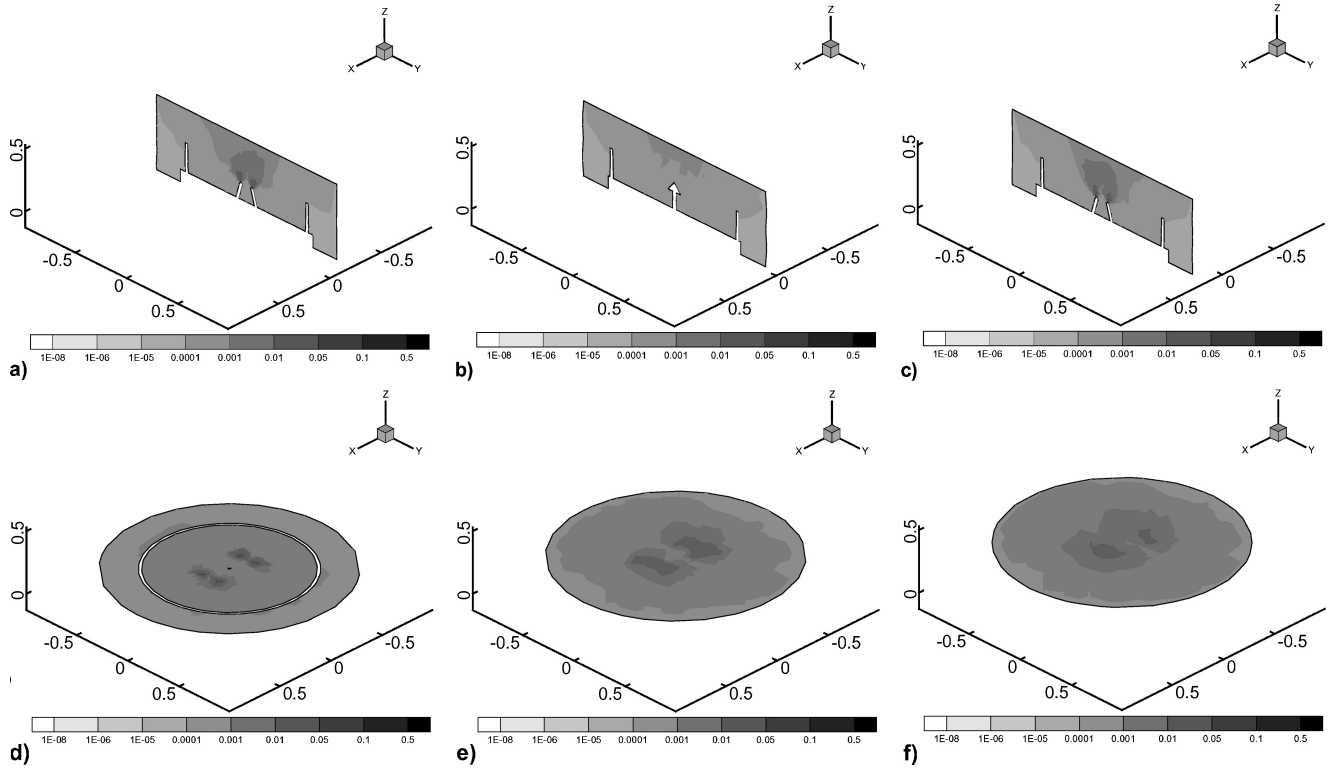

Fig. 7 Distribution of density (kilograms per cubic meter) in the satellite base region for case A: a) $x = -0.18$ m, b) $x = 0$ m, c) $x = 0.18$ m, d) $z = 0.2$ m, e) $z = 0.3$ m, and f) $z = 0.4$ m.

Table 4 Operating conditions considered

Case	TH1P	TH2P	TH3P	TH4P
A	On	On	On	On
B	On	On	Off	Off
C	On	Off	On	Off
D	On	Off	Off	On

The present DSMC computations do not include the flow inside the thruster nozzle; that is, the nozzle exit is regarded as particle source. The Knudsen number at the nozzle exit is computed based on the exit diameter. The nozzle exit properties, as shown in Fig. 4, indicate that the thruster nozzle exit flow can be considered to be near continuum. Therefore, the DSMC approach is used over the whole base region, rather than by division of this region into separate continuum and rarefied regimes. The computational domain consists of about 120,000 cells and the number of simulated particles amounts to about 320,000 at steady state. However, a large number of computing cells is concentrated in the central area to resolve the plume/plume interaction there accurately. A sufficient number of molecules per cell ($\geq$10) is maintained in the central region of the flow, and flow properties are averaged over a large number of sampling steps ($N_{\text{smp}} = 5000$) to minimize statistical scatter. The domain is divided into several subdomains for parallel implementation accordingly. The time step is selected as $\Delta t = 7.5 \times 10^{-8}$ s, and this value is sufficiently small compared to the collision time in every computational cell. Steady state is typically accomplished after 5000 transient steps. An additional 10,000 sampling steps are conducted to obtain the time-averaged flow properties. All of the solid boundaries in the base region are modeled as a diffusely reflected surface with complete energy accommodation. The microscopic properties of participating species are taken from those in Bird's text.[3] The simulated particles are initially introduced through the firing thrusters and spread over the empty space. As indicated in the preceding section, ASTRIUM-France's equilibrium Navier–Stokes simulation data for the MRE-1 thruster are used as the nozzle exit conditions for DSMC computation.

Figure 7 shows the density distributions in the base region for case A. Because the vacuum environment is assumed, all four thruster plumes expand rapidly near the thruster nozzle tip. Because of the blockage by the surrounding ring, most combustion products are distributed inside the base region where the z coordinate is shorter than the height of the surrounding ring, and then expand primarily downward in the $+z$ direction, whereas only a tiny amount of the gas stream moves toward the upper parts of the satellite. As they spread out along the downstream direction, each exhaust plume merges with the adjacent one. Thereby, two-high density zones appear inside the base region as seen in Fig. 7d. The one in the $+x$ side is formed by the plumes from thruster 1P (TH1P) and thruster 4P (TH4P), whereas the other in the $-x$ side is from thruster 2P (TH2P) and thruster 3P (TH3P). The two-high density zones formed inside the base region are again combined in the outside of the base region, where the z coordinate is longer than the height of the surrounding ring (Figs. 7e and 7f). In the engineering approach by ASTRIUM-France, these plume/plume interactions cannot be taken into consideration, and they may lead to lower accuracy in the analysis of a practical application.

Figure 8 shows a distribution of translational temperature for case A. Because a large number of molecules reside inside the base region, the translational temperature there does not diminish significantly with respect to the exit value. A high temperature of over 400 K is found in the vicinity of the S-band antenna cone, along the x axis, due to the strong molecular stream from the nearby high-density zones. Although not shown here, the distribution of rotational temperature is qualitatively similar to that of the translational one.

The density distribution strongly affects the surface properties, such as pressure and heat flux distribution. Figure 9 shows surface heat flux distribution for case A. Figure 9 consists of distributions on five components as follows: 1) S-band antenna and four thrusters

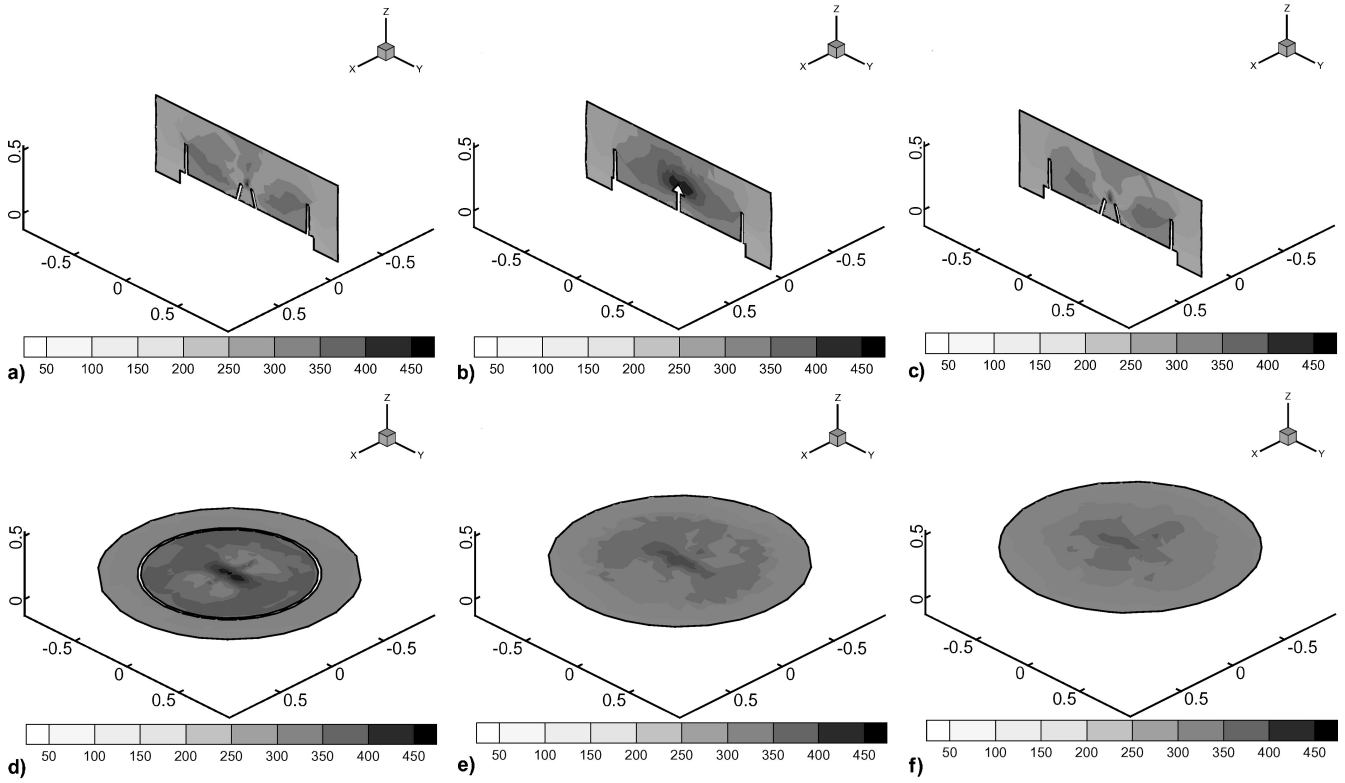

Fig. 8 Distribution of translational temperature (kelvin) in the satellite base region for case A: a) $x = -0.18$ m, b) $x = 0$ m, c) $x = 0.18$ m, d) $z = 0.2$ m, e) $z = 0.3$ m, and f) $z = 0.4$ m.

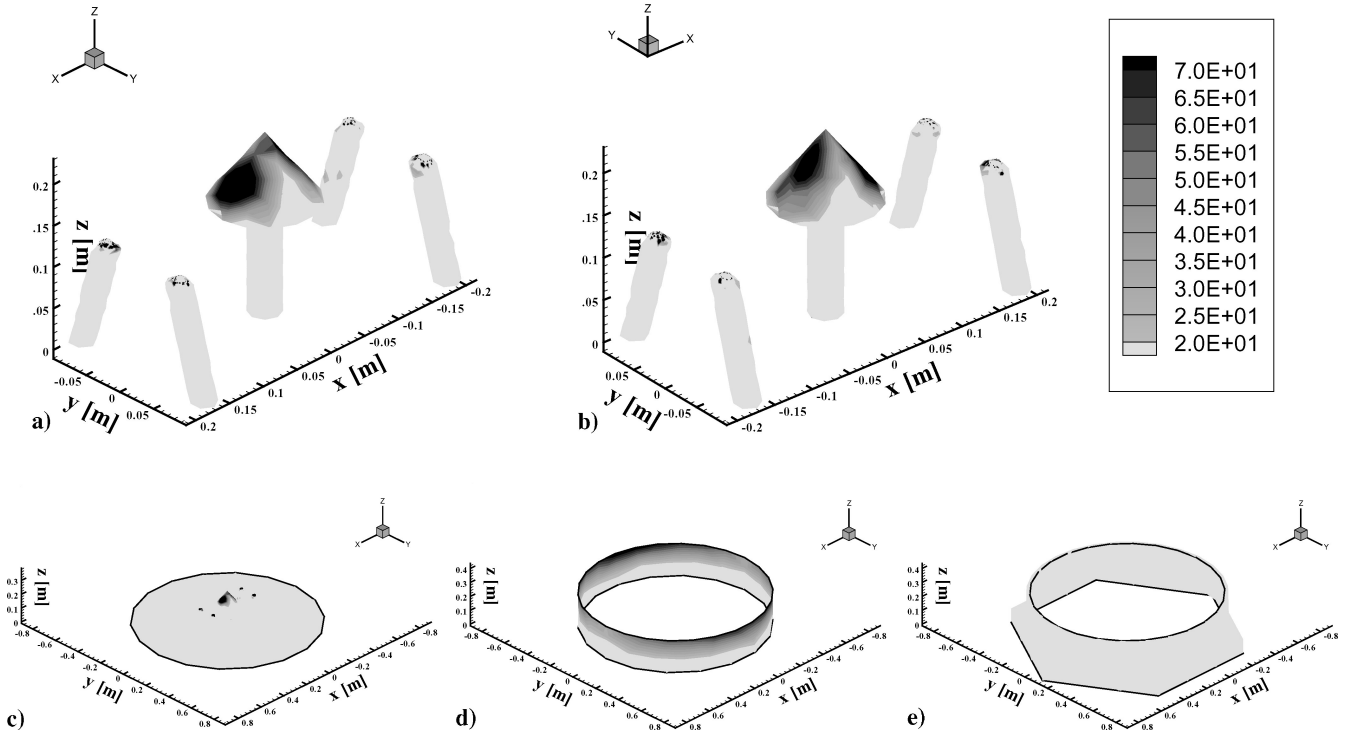

Fig. 9 Distribution of wall heat flux (watts per square meter) in the satellite base region for case A: a) three-dimensional view (+x), b) three-dimensional view (−x), c) three-dimensional view with base plate, d) surrounding ring, inside, and e) surrounding ring, outside.

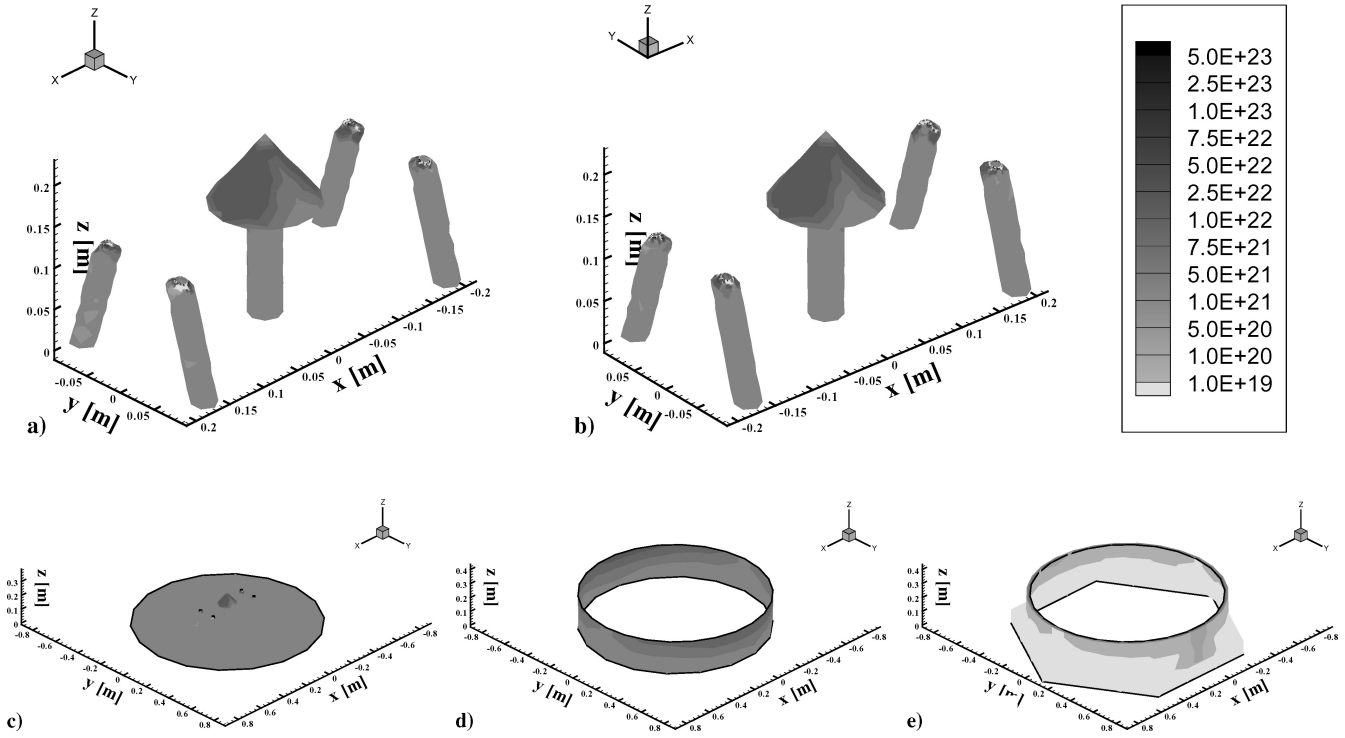

Fig. 10 Surface distribution of wall species H_2 number (per second square meter) flux in the satellite base region for case A: a) three-dimensional view ($+x$), b) three-dimensional view ($-x$), c) three-dimensional view with base plate, d) surrounding ring, inside, and e) surrounding ring, outside.

Table 5 Maximum values of wall properties for various operating conditions for maximum wall heat flux, watts per square meter

Case	S-band antenna	Inner surrounding ring
A	90.65	77.05
B	52.75	69.50
C	58.59	58.52
D	88.24	51.29

Table 6 Maximum values of wall properties for various operating conditions for maximum number flux, number per second square meter

Case	S-band antenna	Inner surrounding ring
A–H_2	1.7626×10^{22}	1.1619×10^{22}
A–N_2	1.1128×10^{20}	3.0890×10^{19}
B–H_2	7.9878×10^{21}	9.1489×10^{21}
B–N_2	4.3066×10^{11}	4.0393×10^{19}
C–H_2	8.8575×10^{21}	7.7215×10^{21}
C–N_2	8.0557×10^{19}	3.8465×10^{19}
D–H_2	1.6425×10^{22}	6.7032×10^{21}
D–N_2	9.7642×10^{19}	2.7360×10^{19}

(viewing from $+x$ side); 2) S-band antenna and four thrusters (viewing from $-x$ side); 3) antenna, thrusters and base plate; 4) inner surrounding ring; and 5) outer surrounding ring. In Fig. 9, whereas two high heat flux zones are observed on the S-band antenna along the x axis, the top periphery of the inner surrounding ring is also heated up along the y axis. The S-band antenna is strongly influenced by the two nearby high-density zones, each of which is generated by a pair of thrusters at the same x location. However, the two thrusters at the same y location mostly affect the inner surrounding ring. In Table 5, the maximum heat fluxes on S-band antenna and inner surrounding ring are compared for the operating conditions in this study. The largest heat flux is found on the S-band antenna in case A, where all four thrusters are fired. However, its value of 100 W/m^2 is quite small compared with the solar constant of $q_{\text{sol}} = 1353$ W/m^2 (Ref. 25). It is, therefore, concluded that the thermal loading, due to impinging plumes on the satellite base region, is negligible.

As described in the preceding section, the exhaust gas consists of three major species of H_2, N_2, and NH_3. Among them, only the distribution of H_2 is presented in Fig. 10 because N_2 and NH_3 are found to be negligible compared with H_2 in the base region. NH_3 is inherently expected to be so because its initial amount in the exhaust mixture is very small, as listed in Table 1. However, for the case of N_2, its negligible quantity is due to species separation. In other words, the light H_2 molecules are remarkably separated from the main stream and expanded diffusely throughout the flow domain, whereas the heavy N_2 molecules reside in the main flow and escape the base area without interfering with satellite structures. Table 6 compares the maximum number fluxes of H_2 and N_2 at the S-band antenna and inner surrounding ring for four cases. Because of species separation, the maximum value for N_2 does not reach 1% of that for H_2. The position of the maximum number flux is almost the same as that of the maximum thermal loading because greater molecular impingement toward the wall can transfer more energy onto the wall. Because in the DSMC results, most of the heat is transported by lighter molecules of H_2, the maximum wall heat flux is smaller than that obtained from the engineering analysis, which models the medium as an overall mixture without the consideration of species composition. For instance, as seen in Table 2, the engineering approach yields the maximum heat flux of 150 W/m^2 when one thruster is fired. However, in the DSMC results, it is still less than 100 W/m^2 even though all four thrusters are simultaneously fired. Consequently, the engineering analysis is considered to have an inherent shortcoming in the investigation of details of the interaction between the thruster plume and the satellite base region. The poor estimation of flow properties may lead to severe error in the design stage.

The final discussion for case A concerns contamination. The capture temperature for H_2 is known to be only 4 K (Refs. 26 and 27).

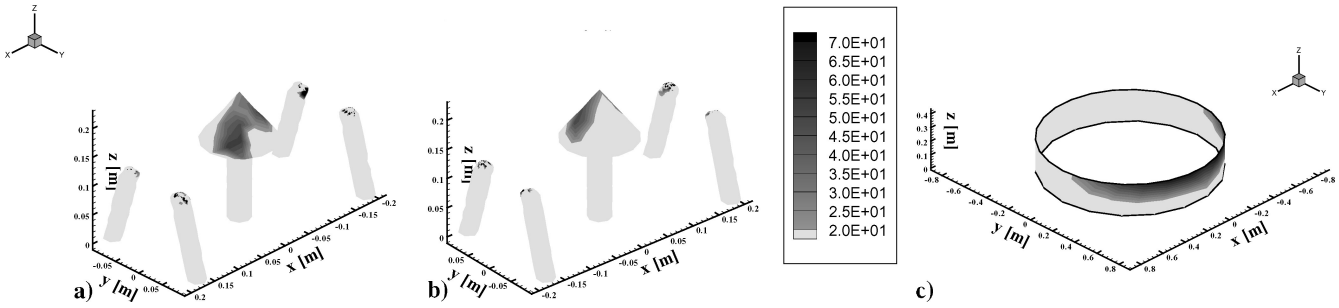

Fig. 11 Distribution of wall heat flux (watts per square meter) in the satellite base region for case B: a) three-dimensional view (+x), b) three-dimensional view (−x), and c) surrounding ring, inside.

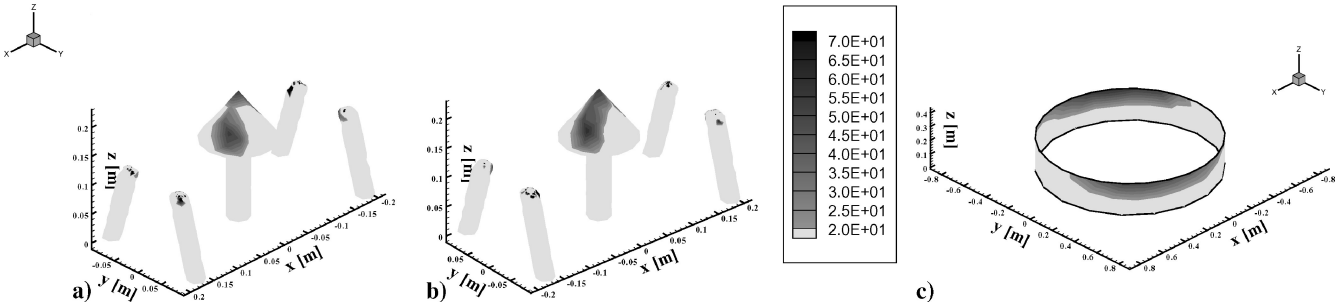

Fig. 12 Distribution of wall heat flux (watts per square meter) in the satellite base region for case C: a) three-dimensional view (+x), b) three-dimensional view (−x), and c) surrounding ring, inside.

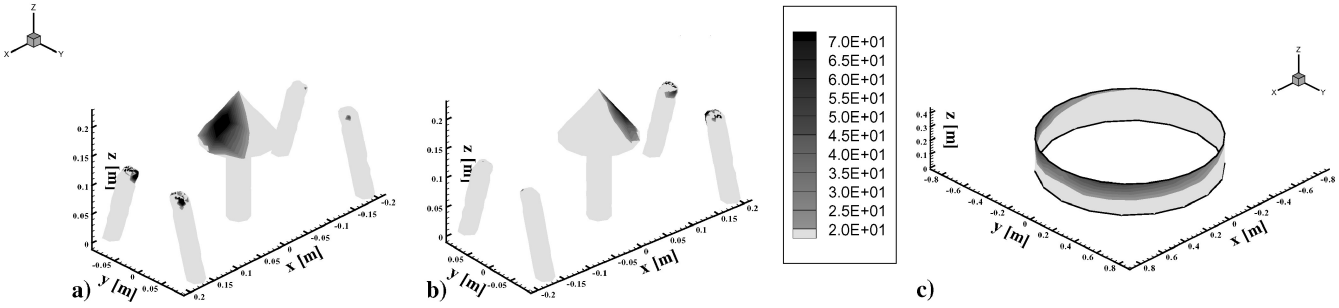

Fig. 13 Distribution of wall heat flux (watts per square meter) in the satellite base region for case D: a) three-dimensional view (+x), b) three-dimensional view (−x), and c) surrounding ring, inside.

The present surface temperatures of the base region are much higher than this even for the worst case. Subsequently, the H_2 molecules are hardly deposited on the solid walls, and the contamination of the satellite base region may be negligible.

Figures 11, 12, and 13 show the distributions of wall heat fluxes for cases B, C, and D, respectively. Similar to case A, the high thermal loading zone is found over the S-band antenna cone, as well as around the periphery of the inner surrounding ring in all cases. Their distributions are strongly dependent on which thrusters are being fired. For cases B, C, and D, the total number of molecules contained in the computing domain is about one-half of that for case A, however, the maximum values of wall heat flux and number flux are not linearly reduced because the interaction between the plumes results in its nonlinear behavior. For case B, in which only the TH1P and TH2P are being fired together, the maximum heat flux on the inner surrounding ring is greater than that on the S-band antenna, whereas the maximum heat flux is almost the same on the inner surrounding ring and S-band antenna for case C, as seen in Tables 5 and 6. As a result, the maximum thermal loading at the surrounding ring and antenna cone is influenced more by the positions of thrusters. Thus, contrary to case B, for case D, in which two close thrusters are being fired, the stronger thermal loading is observed on the antenna cone. For case D, although the total number of occupied molecules is one-half of that for case A, the maximum number flux is close to that for case A. Note that the molecular number flux impinging on the hardware surface is closely related to the thermal loading therein.

Tables 7 and 8, list the disturbance force and torque and their percentage ratios to the nominal values, respectively. All of the ratios are found to be less than 4.1%. Such levels are known only rarely to influence the main satellite dynamics and propellant budget. Based on this, it can be judged that the DTM equipped in KOMPSAT-II are properly arranged to minimize the disturbance effects caused by the plume.

Table 7 Disturbance force/torque vs nominal thrust/torque for various operating conditions

Parameter	x	y	z
	Case A		
Nominal thrust, N	0	0	12.536
Disturbance force, N	1.823×10^{-2}	1.009×10^{-2}	-2.3×10^{-4}
Nominal torque, N · m	2.407×10^{-2}	-0.1226	0
Disturbance torque, N · m	-1.817×10^{-3}	4.297×10^{-3}	2.041×10^{-3}
	Case B		
Nominal thrust, N	0	-1.5628	6.286
Disturbance force, N	5.21×10^{-3}	1.9849×10^{-3}	2.3647×10^{-5}
Nominal torque, N · m	2.0063	-6.1301×10^{-3}	-1.5284×10^{-2}
Disturbance torque, N · m	3.5857×10^{-3}	9.9724×10^{-3}	-9.6059×10^{-4}
	Case C		
Nominal thrust, N	0	0	6.286
Disturbance force, N	6.281×10^{-3}	3.8048×10^{-3}	1.4126×10^{-5}
Nominal torque, N · m	1.203×10^{-2}	-6.1301×10^{-3}	-2.8130×10^{-1}
Disturbance torque, N · m	-6.022×10^{-4}	3.368×10^{-3}	2.087×10^{-3}
	Case D		
Nominal thrust, N	0	0	6.286
Disturbance force, N	1.24×10^{-2}	6.989×10^{-3}	-3.3×10^{-4}
Nominal torque, N · m	1.203×10^{-2}	-1.1895	0
Disturbance torque, N · m	1.985×10^{-3}	1.6094×10^{-3}	6.103×10^{-4}

Table 8 Percentage ratio of disturbances to their nominal values

Case	Thrust, %	Torque, %
A	0.17	4.1
B	0.09	0.53
C	0.12	1.4
D	0.23	0.22

Conclusions

In this study, a DSMC analysis of the interaction between the exhaust plumes and the satellite base region has been performed. To this end, a three-dimensional DSMC code was developed by the use of an unstructured grid system and validated by comparison with experimental meaasurements and other DSMC calculations. This DSMC code was then applied to the analysis of the KOMPSAT-II base region with four hydrazine thrusters, S-band antenna, and inner and outer surrounding rings. With dependence on the combination of firing thrusters, four operating conditions were considered. For each case, the detailed flowfield and surface properties were visualized, and the resultant undesirable effects such as the disturbance force/torque and thermal loading were estimated and discussed. Heat flux due to molecule impingement was found to be significant on both the inner surrounding ring and S-band antenna. Their maximum value was totally dependent on the degree of plume/plume interaction determined by the thruster position. However, the quantitative comparison concluded that the disturbance force/torque, as well as thermal loading, were all negligible with respect to their nominal thrust/torque and solar heating. In other words, the placement of the DTM is such that undesirable effects by plume interaction are expected to be small and within tolerable levels. Among three species in the exhaust gas, only considerable amounts of H_2 were observed to reach the S-band antenna, because of species separation effects. However, H_2 deposition onto the cone surface hardly occurred because the surface temperature was too high to capture H_2 molecules. Furthermore, it was also found that the maximum heat flux estimated from an engineering analysis was higher than that from the DSMC computation.

Acknowledgments

The authors gratefully acknowledge the financial support of the Agency for Defense Development and the Center for ElectroOptics at the Korea Advanced Institute of Science and Technology.

References

[1]Boyd, I. D., and Stark, J. P. W., "Modeling of a Small Hydrazine Thruster Plume in the Transition Flow Regime," *Journal of Propulsion and Power*, Vol. 6, No. 2, 1990, pp. 121–126.

[2]Puyoo, O., Theroude, C., and Chèoux-Damas, P., "Plume Impingement Analysis on the KOMSAT-2 Spacecraft," ASTRIUM, MOS.NT.OP.3682752.01, Toulouse, France, Feb. 2002.

[3]Bird, G. A., *Molecular Gas Dynamics and the Direct Simulation of Gas Flows*, Clarendon, Oxford, 1994.

[4]Boyd, I. D., Penko, P. F., Meissner, D. L., and DeWitt, K. J., "Experimental Investigations of Low Density Nozzle and Plume Flows of Nitrogen," *AIAA Journal*, Vol. 30, No. 10, 1992, pp. 2453–2461.

[5]Chung, C. H., Kim, S. C., and Stubbs, R. M., and DeWitt, K. J., "Low-Density Nozzle Flow by the Direct Simulation Monte Carlo and Continuum Methods," *Journal of Propulsion and Power*, Vol. 11, No. 1, 1995, pp. 64–70.

[6]Lumpkin, III, F. E., Stuart, P. C., and LeBeau, G. J., "Enhanced Analysis of Plume Impingement During Shuttle–Mir Docking Using a Combined CFD and DSMC Methodology," AIAA Paper 96-1877, June 1996.

[7]Rault, D. F. G., "Methodology for Thruster Plume Simulation and Impingement Effects Characterized Using DSMC," AIAA Paper 95-2032, June 1995.

[8]Giordano, D., Ivanov, M., Kashkovsky, A., Markelov, G., Tumino, G., and Koppenwallner, G., "Application of Numerical Multizone Approach to the Study of Satellite Plumes," *Journal of Spacecraft and Rockets*, Vol. 35, No. 4, 1998, pp. 502–508.

[9]Gatsonis, N. A., Nanson, R. A., and Lebeau, G. J., "Simulations of Cold-Gas Nozzle and Plume Flows and Flight Data Comparisons, *Journal of Spacecraft and Rockets*, Vol. 37, No. 1, 2000, pp. 39–48.

[10]Koppenwallner, G., Johannsmeiwe, D., Klinkrad, H., Ivanov, M., and Kashkowski, A., "A Rarefied Aerodynamic Modelling System for Earth Satellites (RAMSES)," *Proceedings of the 19th International Symposium on Rarefied Gas Dynamics*, edited by J. Harvey and G. Lord, Oxford Univ. Press, Oxford, 1995, pp. 1366–1372.

[11]Matting, F. W., "Approximate Bridging Relation in the Transitional Regime Between Continuum and Free-Molecular Flows," *Journal of Spacecraft and Rockets*, Vol. 8, No. 1, 1971, pp. 35–40.

[12]Mayer, E., Hermel, J., and Rogers, A. W., "Thrust Loss Due to Plume Impingement Effects," *Journal of Spacecraft and Rockets*, Vol. 23, No. 6, 1986, pp. 554–560.

[13]Mirels, H., and Mullen, J. F., "Expansion of Gas Clouds and Hypersonic Jet Bounded by a Vacuum," *AIAA Journal*, Vol. 1, No. 3, 1963, pp. 596–602.

[14]Markelov, G. N., Kashkovsky, A. V., and Ivanov, M., "Space Station Mir Aerodynamics Along the Descent Trajectories," *Journal of Spacecraft and Rockets*, Vol. 38, No. 1, 2001, pp. 43–50.

[15]Dietrich, S., and Boyd, I. D., "Scalar and Parallel Optimized Implementation of the Direct Simulation Monte Carlo Method," *Journal of Computational Physics*, Vol. 126, 1996, pp. 328–342.

[16]Kewley, D. J., "Predictions of the Exit Conditions, Including Species Concentrations and the Ratio of, Specific Heats of Hydrazine Decomposition Thrusters," DFVLR, Internal Rept. IB 222-85 A05, Göttingen, Germany, 1985.

[17]"GRIDGEN User Manual," ver. 13.3, Pointwise, Inc., Fort Worth, TX, 1997.

[18]Gropp, W., and Lusk, E., "User's Guide for mpich: a Portable Implementation of MPI," Argonne National Lab., ANL/MCS-TM-ANL 96/6, Argonne, IL, 1996.

[19]Karypis, G., and Kumar, V., "METIS: A Software Package for Partitioning Unstructured Graphs, Partitioning Meshes, and Computing Fill-Reducing Orderings of Sparse Matrices," Dept. of Computer Science and Engineering, Univ. of Minnesota, Minneapolis, MN, Sept. 1998; also URL: http://www.cs.umn.edu/~karypis [cited 26 April 2004].

[20]Hyakutake, T., and Nishida, M., "DSMC Simulation of Parallel, Oblique, and Normal Free Jet Impingements on a Flat Plate," *Transactions of Japan Society of Aeronautics and Space Science*, Vol. 43, No. 139, 2000, pp. 1–7.

[21]Kannenberg, K. C., and Boyd, I. D., "Three-Dimensional Monte Carlo Simulations of Plume Impingement," *Journal of Thermophysics and Heat Transfer*, Vol. 13, No. 2, 1999, pp. 226–235.

[22]Chèoux-Damas, P., and Koeck, C., "Thermal Effects of Plume Impingement," *Proceedings of the 3rd European Symposium on Space Thermal Control and Life Support Systems*, SP-288, ESA, Noordwijk, The Netherlands, 1988, pp. 273–279.

[23]Theroude, C., Maag, M.-C., and Chèoux-Damas, P., "Spacecraft/Thrusters Interaction: New Models for Chemical Propulsion," *Proceedings of 3rd International Conference on Spacecraft Propulsion*, SP-465, ESA, Noordwijk, The Netherlands, 2000, pp. 609–618.

[24]Kim, J. S., "Technical Information on Input and Requirements for Output Generation: Plume Analysis, KOMPSAT-II," Korea Aerospace Research Inst., KS-D0-460-010, Taejon, Republic of Korea, Oct. 2001.

[25]Modest, M. F., *Radiative Heat Transfer*, McGraw–Hill, New York, 1993, Chap. 1.

[26]Barewald, R. K., and Passamaneck, R. S., "Monopropellant Thruster Plume Contamination Measurements," Jet Propulsion Lab., JPL Publication, California Inst. of Technology, Pasadena, CA, Sept. 1997.

[27]Chèoux-Damas, P., Theroude, C., and Ounougha, L., "Contamination Modelling in Space Environment," *Proceedings of the 6th International Symposium on Material in a Space Environment*, SP-368, ESA, Noordwijk, The Netherlands, 1994, pp. 45–50.

C. Kaplan
Associate Editor